UNIVERSITY OF MICHIGAN

Effects of transient topography and drainage basin evolution on detrital thermochronometer data

by Eleanor Ferguson

Submitted to the Department of Geological Sciences in Partial Fulfillment of the

Requirements for the Honors Bachelor of Science in Earth Systems Science

April 22, 2009

Research Advisor: Todd A. Ehlers
tehlers@umich.edu
University of Michigan
Department of Geological Sciences

Contents

Acknowledgments

I am indebted to my advisor, Professor Todd Ehlers, for accepting me into his research group and making this thesis possible. I would especially like to thank Todd for his unfaltering patience, his confidence in me and his invaluable advice regarding all aspects of this project as well as my academic life in general. I am also grateful to the whole Earth Surface Processes Research Group for their support and for making work even more fun. Last I would like to thank Mom, Dad, Jeff, Alex and Gram for always being there for me.

Abstract

Understanding how mountain ranges evolve is important for interpreting the geologic and topographic history of orogens. Quantifying the topographic evolution of orogens is difficult because the rates and processes involved occur over long timescales. Detrital thermochronometer data has the potential to quantify landscape evolution. Understanding the sensitivity of detrital thermochronometer data to topography, erosion and other factors allows geologists to use the data to interpret the history of mountain belts. This study focuses on the effects of evolving topography and erosion on the age distributions that would be found in a sedimentary basin below a mountain belt. This study presents results from a series of coupled numerical models (Pecube and Cascade) used to simulate the thermochronometer response to topographic evolution of different wavelengths and amplitudes. The thermokinematic model Pecube calculates the history of rocks exposed at the surface after erosion and evolving topography. Free parameters include crustal thickness, density, thermal diffusivity, and radiogenic heat production. The program solves equations describing the changes in height for each position across the topography, taking into account both tectonic and erosional processes. Changing topography is calculated using the surface process model Cascade, which accounts for fluvial and hillslope processes. The thermal histories from rocks exhumed to the Earth surface are used to predict mineral cooling ages as a function of the topographic history of the mountain range. The results of simulations testing different exhumation rates and rates of drainage basin evolution show a potential signal of topographic evolution in detrital thermochronometer data.

1. Introduction

Detrital thermochronometer data have the potential to quantify the history of landscape evolution and transient topography in a mountain belt because topography deflects isothermal surfaces in the crust (Mancktelow and Grasemann 1994, House *et al.* 1998). Topography has the greatest effect on the thermal field in the upper few kilometers of the crust, so a thermochronometer with a low closure temperature has the most potential for recording the effects of transient topography (House *et al.*, 1998). For this reason, we make predictions for the low temperature thermochronometers apatite (U-Th/He) and apatite fission track. Detrital cooling ages sampled in modern rivers or sedimentary basins are effected by evolving topography, erosion, wildfires, groundwater and other factors that may deflect the geothermal field (Whipp *et al.*, in press 2009). It is important to understand the sensitivity of detrital thermochronometer data to these factors in order to accurately interpret the history of a mountain belt. The goal of this paper is to quantify the effects of evolving topography and erosion on the age distributions that would be found in a sedimentary basin downstream of the mountain belt.

Previous work addressing the effect of drainage basin evolution on mineral cooling ages has been limited. A study by Whipp *et al.* (in press 2009) has looked at the effect of changing relief on detrital thermochronometer data in different kinematic scenarios. Rahl *et al.* (2007) evaluated transient erosion rates recorded in detrital data using a one-dimensional numerical model to make predictions for detrital thermochronometer ages. Their study confirmed that detrital thermochronology can be used to quantify erosion rates, but did not evaluate drainage basin evolution. Ruhl and Hodges (2005) used modern river sediments to quantify erosion rates, but did not evaluate evolving topography or transient erosion rates, instead assuming steady state topography during the closure interval recorded by the detrital thermochronometer ages. Brewer and Burbank (2003) compared $^{40}Ar/^{39}Ar$ muscovite age distribution data with predictions of a numerical model that assumed a time invariant erosion rate. Brewer and Burbank (2006) evaluated the influence of faulting geometry on detrital ages using numerical models of erosion in collisional orogens that assumed topographic steady state. Studies by House *et al.* (1998) and Ehlers *et al.* (2006) were more observational in scope and sought to document observed cooling age signals of changing topography.

This project complements previous studies by attempting to quantify the influence of drainage basin evolution on detrital thermochronometer signals observed in sedimentary basins. Our approach utilizes a series of coupled numerical models including a landscape evolution model, 3D thermal model and a cooling rate dependent age prediction model. The results of simulations testing different exhumation rates show that there is potential to find a signal of topographic evolution in detrital thermochronometer data.

2. Model setup

This study utilizes coupled thermokinematic and surface process models to simulate topographic evolution and calculate the cooling history of rocks exposed at the Earth's surface. We employed a version of the thermokinematic model Pecube (Braun, 2003) modified to predict cooling age distributions in drainage basins. Figure 1 illustrates the parameters and processes included in the numerical models. Details of each of the models are as follows.
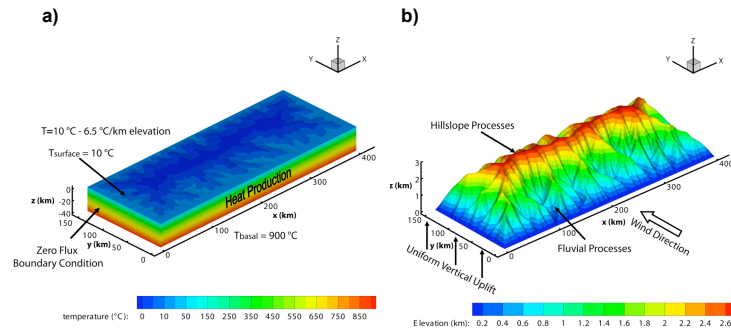
Figure 1. (a) Thermal model setup includes a zero flux boundary condition, basal temperature of 900°C, heat production and surface temperature boundary condition of 10°C. The atmospheric thermal gradient is -6.5°C/km of elevation. (b) The surface process model includes hillslope and fluvial erosional processes and imposed uniform vertical uplift from the coupled kinematic model. The model also includes spatial climatic variations such as wind direction, temperature and precipitation.

Table 1: Model Parameters

Property/Parameter	Model Input Value	Symbol
Material Properties		
Volumetric radiogenic heat production	2.5 μW/m^3	A
Heat production e-folding depth	10 km	
Thermal conductivity	2.5 W/m K	k
Specific heat capacity	1000 J/kg K	c
Crustal density	0.25 kg/m^3	ρ_c
Mantle density	15 kg/m^3	ρ_m
Range of Thermal Model Parameters Considered		
Vertical rock uplift rate (0-50 Myr)	0.00 – 0.1 mm/yr	$\vec{v}$
Vertical rock uplift rate (50-70 Myr)	0.25 – 1.5 mm/yr	$\vec{v}$
Model time step	Dynamic	
Horizontal node spacing	1000 m	
Average vertical node spacing	1000 m	
Basal temperature	900 °C	T_{basal}
Model domain	400 × 150 × 40 km	

Surface Process Model and Atmospheric Parameters		
Fluvial erosion constant	2·10^{-4} m^{-1}	k_f
Bedrock erosion length scale	1000 m	
Diffusion constant	20 m^2/yr	k_d
Surface temperature at lowest elevation	10 °C	$T_{surface}$
Atmospheric lapse rate	-6.5 °C/km	Γ
Background moisture content	0.3 m/yr	a_0
Moisture gradient	110 m/yr per (m/s)	a_1
Variance in atmospheric vertical velocity	1/.01 m/s	
Average wind speed	0.8 m/s	
Cross wind smoothing scale	50 km	
Upwind smoothing scale	50 m	

2.1 Thermokinematic model

We utilize the thermokinematic numerical model Pecube (Braun, 2003), modified to predict age distributions for different thermochronometers (Whipp *et al.*, in press 2009). This model was used to simulate the processes of topographic evolution potentially recorded in thermochronometer data from sedimentary basins. The model has two main components: a kinematic model and a thermal model. The following sections describe the numerical model setup and the free parameters.

2.1.1 Kinematic model

The kinematic model simulates rock transport from erosional exhumation. We focus on a scenario of imposed uniform vertical uplift with varying exhumation rates. The kinematic and thermal models were started 50 Myr prior to the surface process model to produce a crustal block with an initial age distribution. The range of initial input velocities considered was 0.00 – 0.1 mm/yr for the first 50 Myr of the simulation (70-20 Ma). All the simulations discussed in this study used an initial uplift velocity of 0.10 mm/yr. After the initial crustal age distribution was

created, the couple thermokinematic and surface process models tested rock uplift velocities in the range 0.25 – 1.5 mm/yr for the last 20 Myr of the simulation (20-0 Ma).

2.1.2 Thermal model

The background thermal state of the crust is determined by heat flow into the base of the crust, the surface temperature, and thermal physical properties such as thermal diffusivity and heat production. In tectonically active areas this background thermal field is perturbed by erosion and sedimentation, topographic evolution, faulting, and lateral variations in thermal properties. Pecube solves the transient advection-diffusion equation using the advection velocity from the kinematic model,

$$\rho_c c \left(\frac{\partial T}{\partial t} + v_x \frac{\partial T}{\partial x} + v_y \frac{\partial T}{\partial y} + v_z \frac{\partial T}{\partial z} \right) = \frac{\partial}{\partial x} k \frac{\partial T}{\partial x} + \frac{\partial}{\partial y} k \frac{\partial T}{\partial y} + \frac{\partial}{\partial z} k \frac{\partial T}{\partial z} + \rho_c A \qquad (1)$$

where ρ_c is the crustal density, c is the specific heat capacity, T is temperature, t is time, $x, y,$ and z are spatial coordinates, $v_x, v_y,$ and v_z are the components of advection velocity from the kinematic model, k is the thermal conductivity, and A is the volumetric radiogenic heat production (Whipp *et al.*, in press 2009). The values considered for the free parameters $\rho, c, T, k,$ and A are listed in Table 1. This equation is solved using upper and lower boundary conditions of constant temperature and zero flux boundary conditions along the sides of the model, as illustrated in Figure 1. The primary output of the thermal model is the thermal history of rocks exposed at the surface, which is used to calculate the cooling-rate dependent apatite helium and fission track ages following the approach of Ehlers *et al.* 2005.

2.2 Surface process model

Topography in orogens develops as rivers cut channels into the bedrock and rivers and hillslope processes, such as diffusion and mass wasting, carry material downhill. Topography and climate form a coupled system controlling erosion rates and orographic evolution. The topography causes orographic precipitation by forcing upward movement of warm, moist air. Climatic variables in turn control river discharge, determining fluvial erosion rates which control the development of topography. The surface process model Cascade calculates the temporal evolution of topography as a function of tectonic uplift and hillslope and fluvial erosion, following the approach of Willett *et al.* 2007 and Braun and Sambridge 1997. Model free parameters include climatic variables and material properties that influence fluvial and hillslope processes described in

Table 1.

Hillslope processes are represented by diffusion, and the change in height in time due to hillslope erosion is calculated using diffusion in two dimensions,

$$\frac{\partial h}{\partial t} = k_d \left(\frac{\partial^2 h}{\partial x^2} + \frac{\partial^2 h}{\partial y^2} \right) \qquad (2)$$

where k_d is a diffusion constant and h is the height at the location x, y at time t (Willett, 2001).

Fluvial erosion depends on the discharge in the river which is calculated using spatial variations in climate, including orographic precipitation and feedback, following the approach of Roe et al. 2002. The change in height over time due to fluvial erosion processes is calculated from the dimensions of the channel and the discharge,

$$\frac{\partial h}{\partial t} = \frac{k_f}{w} Q \frac{\partial h}{\partial l} \qquad (3)$$

where w and l are the width and length of the channel, k_f the fluvial erosion constant and Q is the discharge (Willett, 2001).

The hillslope and fluvial erosion equations are combined with an applied uniform uplift u, giving an equation for the change in height,

$$\frac{\partial h}{\partial t} = u + k_d \left(\frac{\partial^2 h}{\partial x^2} + \frac{\partial^2 h}{\partial y^2} \right) + \frac{k_f}{a} \sqrt{Q} \frac{\partial h}{\partial l} \tag{4}$$

where a is a proportionality constant accounting for the stream width (Willett, 2001)

The primary output of the surface process model is the change in elevation across the domain as a function of time. The changing topographic surface, and hence erosion rates, are used as the top boundary condition in the thermal model such that mineral cooling ages are calculated as a function of the topographic evolution.

3. Results

A wide range of thermal and surface process parameters were considered (as shown in Table 1) to simulate the sensitivity of thermochronometer systems to different rates of topographic evolution. For simplicity a subset of these results is presented, for the cases where the thermochronometer signal of topographic evolution was most pronounced.

3.1 Influence of uplift on drainage basin evolution

Figure 2 presents the results of two simulations with exhumation rates of 0.25 mm/yr and 1.00 mm/yr. The primary feature here is the change in relief over time. In both scenarios the relief grows through time and eventually reaches equilibrium. The evolution of topographic relief is presented in Figure 3. For example, Figure 2 shows that after 2 Myr of uplift the topography has a relief of 0.6 km for a simulation with an exhumation rate of 0.25 mm/yr. After 7 Myr, simulation a) has reached steady state and relief stays constant for the next 13 Myr (as seen in Figure 3). Figures 2 and 3 also show that relief grows more quickly for faster exhumation rates. Simulations at 0.25 mm/yr and 1.00 mm/yr both reached steady state topography at approximately 7-10 Myr, but the 1.00 mm/yr simulation reached a steady state elevation more than three times that of the slower rate.

The change in basin size as topography evolves is the second important feature displayed in Figure 2. Inspection of Figure 2 a) shows that drainage basins roughly double in size between 2 and 5 Myr. The rate of basin evolution is primarily controlled by the efficiency of fluvial processes. Rates of fluvial erosion depend on local channel slopes, discharge, and climate (e.g. Eqn. 3). Higher uplift rates generate steeper channel slopes and a higher orographic precipitation and therefore erode more quickly.
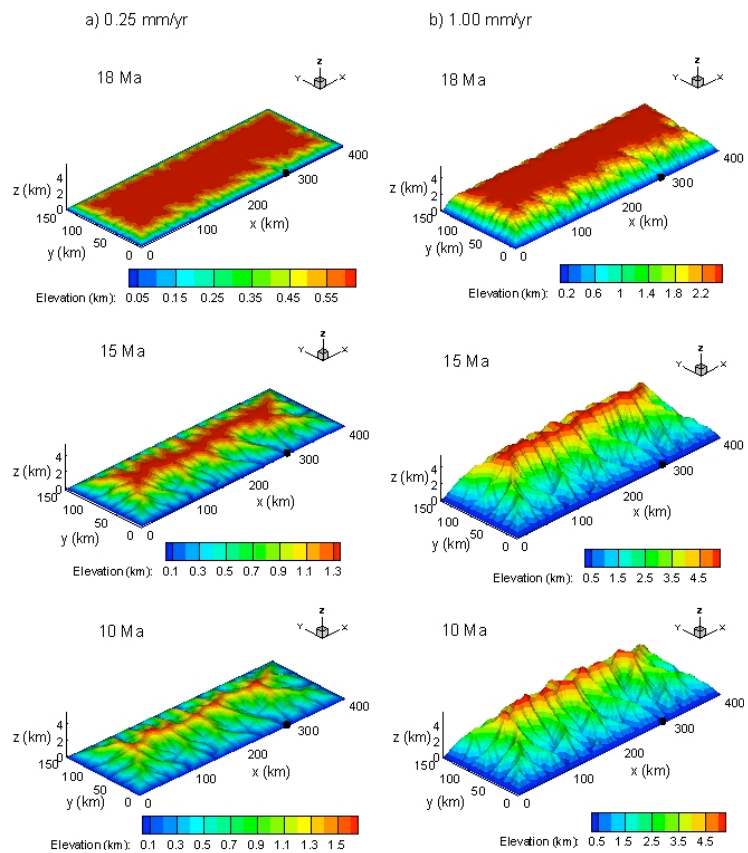
a) 0.25 mm/yr

18 Ma

Elevation (km): 0.05 0.15 0.25 0.35 0.45 0.55

15 Ma

Elevation (km): 0.1 0.3 0.5 0.7 0.9 1.1 1.3

10 Ma

Elevation (km): 0.1 0.3 0.5 0.7 0.9 1.1 1.3 1.5

b) 1.00 mm/yr

18 Ma

Elevation (km): 0.2 0.6 1 1.4 1.8 2.2

15 Ma

Elevation (km): 0.5 1.5 2.5 3.5 4.5

10 Ma

Elevation (km): 0.5 1.5 2.5 3.5 4.5

Figure 2. Influence of rock uplift rate on drainage basin evolution. Contour plots of elevation are shown at 18 Ma, 15 Ma and 10 Ma for rock uplift rates of (a) 0.25 mm/yr and (b) 1.00 mm/yr. (a) The topography reaches a steady state with an elevation of approximately 1.7 km between 15 and 10 Ma. (b) The faster exhumation rate causes the topography to develop more rapidly and the steady state elevation of approximately 5 km is reached by 10 Ma. The black

points mark the location of catchment 1394 which will be discussed in detail in section 4. Results for part a) are from simulation m026c, and m029c for b).
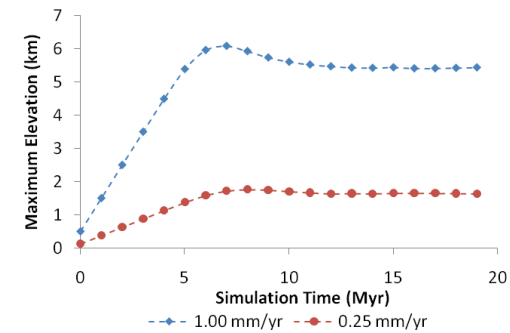

Figure 3. Effect of varying rock uplift rates on topographic evolution. Results of simulations with rock uplift rates of 1.00 mm/yr and 0.25 mm/yr are shown. Both reach steady state topography between 5 and 10 Myr. Results for the uplift rate of 0.25 mm/yr are from simulation m026c, and results for 1.00 mm/yr are from m029c.

Figure 4a) illustrates the development of the catchment labeled with a black point in

Figure 2. The catchment develops rapidly early in the simulation and reaches a steady state by

15 Myr. Figure 4b) shows the migration of the drainage divide as topography develops. At the

beginning of the simulation (0 Myr) the drainage divide is symmetric at 50% of the domain and

when the topography reaches equilibrium the divide has advanced to between 60 and 70% of the

domain. Migration of the drainage divide indicates that the size of the drainage basin is

changing the most during the first approximately 7 Myr and then reaches steady state.

Figure 4a. Schematic of catchment development for catchment 1394 (indicated with a black point in Figures 2 and 5) in simulation m026c (0.25 mm/yr). The catchment grows rapidly at the beginning of the simulation (between 2 and 5 Myr), and reaches a steady state by 10 Myr.
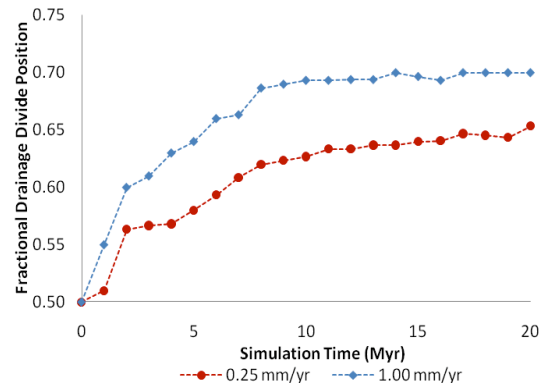

Figure 4b. The fluvial drainage basin divide position as a function of simulation duration. Results are shown for simulations with rock uplift rates of 0.25 mm/yr and 1.00 mm/yr. In both cases, the divide position advances until it reaches equilibrium. This average divide position of all basins was measured from y=0 as it progressed across the domain. Results for the uplift rate of 0.25 mm/yr are from simulation m026c, and results for 1.00 mm/yr are from m029c.

3.2 Influence of drainage basin evolution on cooling ages

Figure 5 shows the apatite (U-Th/He) ages of rocks exposed at the surface as two simulations progress. The first order trend apparent in Figure 5 is that the age range varies in time. For example, 2 Myr into the simulation of topographic evolution (18 Ma), the age ranges are small (~7 Myr for 0.25 mm/yr) and not much topographic relief has developed (0.5 km for 0.25 mm/yr, from Figure 3). As relief grows, the legends show that the age ranges increase. Eventually the age ranges begin to decrease in time. The second order trend that appears in Figure 5 is an age range dependence on exhumation rate. For example, a simulation with a fast uplift rate of 1.5 mm/yr reaches a maximum age range for rocks exposed at the surface at approximately 5 Myr while a simulation with a slower uplift rate of 0.25 mm/yr reaches a maximum age range later at approximately 8 Myr. This can be seen more quantitatively in Figure 6 where the age-range exposed at the surface is plotted as a function of simulation duration. The initial age distribution in the simulation causes the initially large range of ages that then decreases. The largest age ranges coincide with the times of topographic development seen in Figure 3.
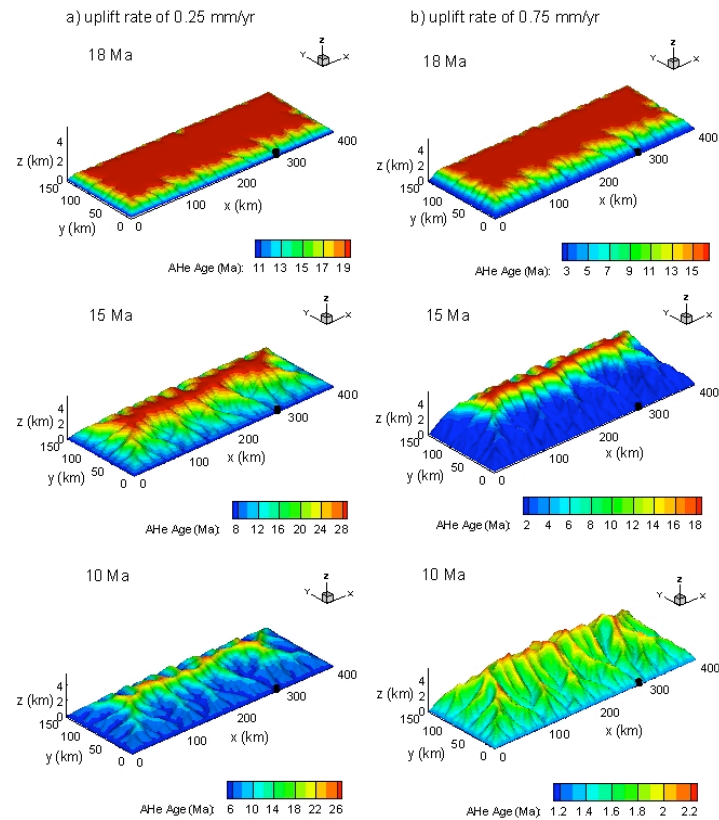
Figure 5. Influence of drainage basin evolution on apatite (U-Th)/He cooling ages. These plots present the ages of rocks exposed at the surface for three different times and for simulations m026c and m028c with respective exhumation rates of 0.25 and 0.75 mm/yr. The contour scales give a sense of the age ranges eroding off the mountain at a time in the simulation. The black point indicates the position of catchment 1394, which will be considered in the discussion section. These plots with apatite fission track are included in the appendix.
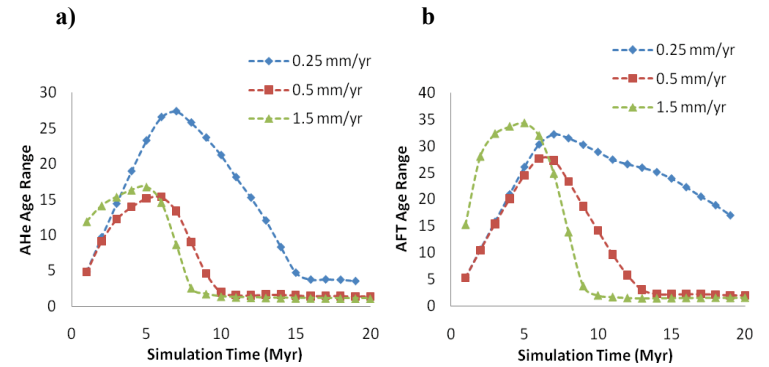
Figure 6. Crustal age ranges over time. These graphs quantitatively illustrate the age ranges shown in Figure 5. a) Apatite (U-Th)/He and b) apatite fission track age ranges of rocks exposed at the surface are presented at different times throughout the topographic development. Results are presented for simulations m026c, m027c and m030c with rock uplift rates of 0.25, 0.5 and 1.5 mm/yr, respectively. For both thermochronometers considered, the simulation with the fastest rock uplift rate reaches a maximum age range first, followed by the intermediate rate, and then the simulation with the slowest exhumation rate.

4. Discussion

4.1 Rates of drainage basin evolution

Rates of drainage basin evolution are controlled by fluvial and hillslope processes. Climatic effects on river discharge control fluvial erosion, while topographic evolution controls hillslope processes and climate feedbacks. Faster uplift rates cause the drainage basin divide to migrate further across the domain, producing faster drainage basin evolution. Precipitation varies with time due to orographic feedbacks. The topographic and climatic feedbacks in the system control the rate of topographic evolution

4.2 General considerations on thermochronometer sensitivity to basin evolution

For a measurable signal of transient topography to appear in detrital data, topography must evolve at a time when a large range in cooling ages is exposed at the surface. A large age range creates greater sensitivity to the amount of area exposed at the surface at different elevations, creating greater sensitivity to catchment evolution. For example, Figure 6 shows that the exhumation rate affects the time that the age range reaches a maximum. This suggests that maximum age ranges will occur at different depths in a stratigraphic column, depending on the exhumation rate. This should make it possible to quantify the exhumation rate of a mountain using detrital data. A larger age range exists for a longer period of time for simulations with lower exhumation rates. The conditions for a signal of transient topography include a large age range during topographic evolution and a slow exhumation rate that allows a large crustal age range to exist throughout topographic development.

The thermochronometer ages of the rocks exposed at the surface are used to calculate synthetic cooling age distributions that would be found in a sedimentary basin. The points on the model that contribute to a certain catchment are determined using the D8 algorithm (Garbrecht and Martz, 1997). An age histogram forms a raw age distribution, with the assumption that every point in the catchment produces sediment that will contribute to the age distribution found in a stratigraphic column downstream (Whipp *et al.*, in press 2009). These raw age distributions are then time shifted to account for the remainder of the simulation time, during which the sediment continues to age in the sedimentary basin. In Figure 7 we estimate the magnitude of the signal by producing synthetic PDFs of cooling ages in a catchment for a simulation with an exhumation rate of 0.25 mm/yr. The catchment considered is indicated with a black point in Figures 2 and 5. There are two considerations that will affect the fidelity of a signal that could

be recovered: 1) Topography must evolve when a large age range exists in the crust, and 2) the inherited age (age range depends on both the uplift rate and the inherited age signal in the crust prior to topographic evolution).

Figure 3 indicates rapid topographic evolution occurs during the first 5-10 Myr of simulations m026c and m030c with uplift rates of 0.25 mm/yr and 1.00 mm/yr. The largest variations in cooling ages in Figure 7 a) occur over the same time period for simulation m026c. This suggests sensitivity to drainage basin evolution. In Figure 7 a), the synthetic cooling age PDFs for 5 Myr and 10 Myr have large age ranges but very different geometries. Figures 7 c) and d) present the age distributions for simulation m030c, which has a faster uplift rate of 1.00 mm/yr. The age ranges narrow before the topography reaches steady state, creating less sensitivity to drainage basin evolution. For slower uplift rates, a large age range exists in the stratigraphic column for a longer period of time, producing a longer record of drainage basin evolution. However, age range and the shape of the distribution may also be sensitive to the initial (inherited) age distribution. Future studies could focus on understanding how these PDFs differ for steady state topography throughout the entire history as compared to transient topography.

A detrital signal of transient topography requires 1) a large initial crustal age range, 2) slow rock uplift rates (~0.25-0.75 mm/yr), 3) low to medium precipitation rates to keep erosion rates low. If the above conditions are met, then basin evolution will occur at time scales of 5-10 Myr in the simulation and will be accompanied by a large age range in sediments preserved in a basin of this age.
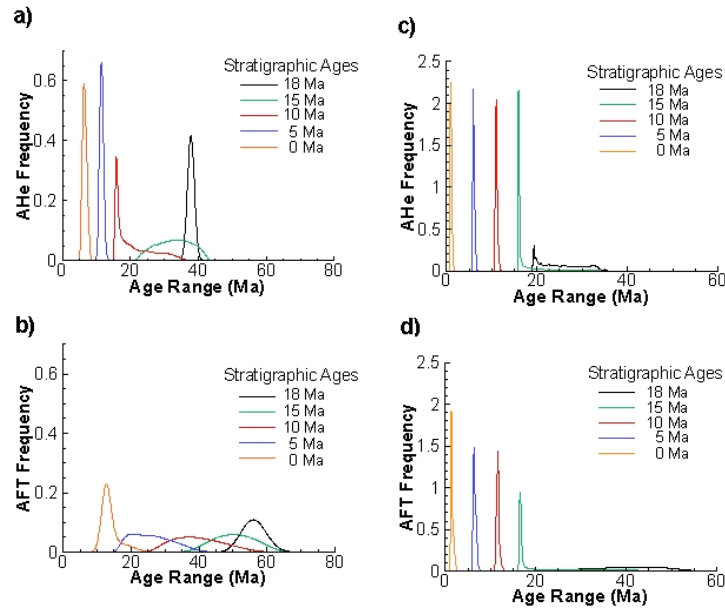
Figure 7. Synthetic probability density functions in catchment 1394 for a) apatite helium ages in simulation m026c with rock uplift rate of 0.25 mm/yr, b) apatite fission track ages in simulation m026c at 0.25 mm/yr, c) apatite helium ages in simulation m030c at 1.00 mm/yr, and d) apatite fission track ages in simulation m030c at 1.00 mm/yr. These plots estimate the magnitude of signal predicted for a PDF of this catchment.

5. Conclusions

This study used 3-D coupled thermokinematic and surface process models to analyze the influence of transient topography on detrital thermochronometry. Topographic evolution occurs between 5-10 Myr for each simulation, and the uplift rate determines the steady state elevation of the topography. Slower uplift rates allow a larger age range to exist on the topography for a longer period of time, due to lower orographic precipitation rates and slower erosion. We found that large age ranges in detrital data indicate periods of rapidly evolving topography. The PDFs of age ranges in a catchment showed narrow age ranges early in topographic development and after the orogens had reached steady state topography for a slow uplift rate. For a faster uplift rate the age range disappeared more quickly, before the orogen reached steady state. There is potential to find a signal of transient topography in detrital thermochronometry data from an orogen with a large initial age range in the crust and a slow exhumation rate.

Thermochronometer data from sedimentary basins could be used as a way to constrain paleotopography. However, the remaining issue of inherited crustal age distribution still needs to be resolved.

6. References

Braun, J., and M. Sambridge (1997), Modelling landscape evolution on geological time scales: a new method based on irregular special descretization, *Basin Res., 9,* 27-52.

Braun, J., P. van der Beek, and G. E. Batt (2006), *Quantitative Thermochronology*, 1 ed., 270 pp., Cambridge University Press.

Brewer, I., and D. W. Burbank (2006), Thermal and kinematic modeling of bedrock and detrital cooling ages in the central Himalaya, *J. Geophys. Res., 111*(B9), B09,409.

Brewer, I., D. W. Burbank, and K. V. Hodges (2003), Modeling detrital cooling-age populations; insights from two Himalayan catchments, *Basin Research, 15*(3), 305-320.

Brewer, I., D. W. Burbank, and K. V. Hodges (2006), Downstream development of a detrital cooling-age signal; insights from [40]Ar/[39]Ar muscovite thermochronology in the Nepalese Himalaya, in *Tectonics, Climate and Landscape Evolution, Penrose Conference Series,* vol. 398, edited by S. D. Willett, N. Hovius, M. T. Brandon, and D. M. Fisher, pp 321-338, Geological Society of America.

Ehlers, T. A. (2005), Crustal thermal processes and the interpretation of thermochronometer data, in Low-Temperature Thermochronology: Techniques, Interpretations, and Applications,

Rev. Mineral. Geochem., vol. 58, edited by P. W. Reiners and T. A. Ehlers, pp. 315–350, Mineral. Soc. of Am., Washington, D.C.

Ehlers, T. A., and K. A. Farley (2003), Apatite (U-Th)/He thermochronometry; methods and applications to problems in tectonic and surface processes, *Earth Planet. Sci. Lett., 206*, 1-14.

Garbrecht, J., and L. W. Martz (1997), The assignment of drainage direction over flat surfaces in raster digital elevation models, *Journal of Hydrology*, *193*(1-4), 204-213.

House, M. A., B. P. Wernicke, and K. A. Farley (1998), Dating topography of the Sierra Nevada, California, using apatite (U-Th)/He age, *Nature*, *396*, 66-69.

Huerta, D. A., L. H. Royden, K. V. Hodges, (1996), Interdependence of deformational and thermal processes in mountain belts, *Science*, *273*, 637-639.

Rahl, J. M., T. A. Ehlers, and B. A. van der Pluijm (2007), Quantifying transient erosion of orogens with detrital thermochronology from syntectonic basin deposits, *Earth and Planetary Science Letters*, *256*(1-2), 147-161.

Roe, G. H., D. R. Montgomery, and B. Hallet (2002), Effects of orographic precipitation variations on the concavity of steady-state river profiles, *Geology, 30,* 143-146.

Roe, G. H., D. R. Montgomery, and B. Hallet (2003), Orographic precipitation and relief of mountain ranges, *J. Geophys. Res., 108*(B6)*,* 2315, doi:10.1029/2001JB001521.

Ruhl, K. W., and K. V. Hodges (2005), The use of detrital mineral cooling ages to evaluate steady state assumptions in active orogens; an example from the central Nepalese Himalaya, *Tectonics*, *24*, no.4, 14.

Willett, S. D., R. Slingerland, and N. Hovius (2001), Uplift, shortening, and steady state topography in active mountain belts, *Am. J. Sci, 301*, 455-485.

Whipp, D. M., T. A. Ehlers, J. Braun (in press 2009), Effects of exhumation kinematics and topographic evolution on detrital thermochronometer data, *J. Geophys. Res.*

Wolf, R. A., K. A. Farley, and L. T. Silver, (1996), Helium diffusion and low temperature thermochronometry of apatite. *Cheochim. Cosmochim. Acta 51*, 2865-2868.

7. Appendix

Figure 8 presents the distribution of precipitation across the model for the simulations shown in Figure 2. The forced advection of warm, moist air causes heavy precipitation on the windward side of the topography, increasing river discharge and fluvial erosion rates.

Figure 9 presents the apatite fission track ages of rocks exposed at the surface for the same simulations shown in Figure 5.
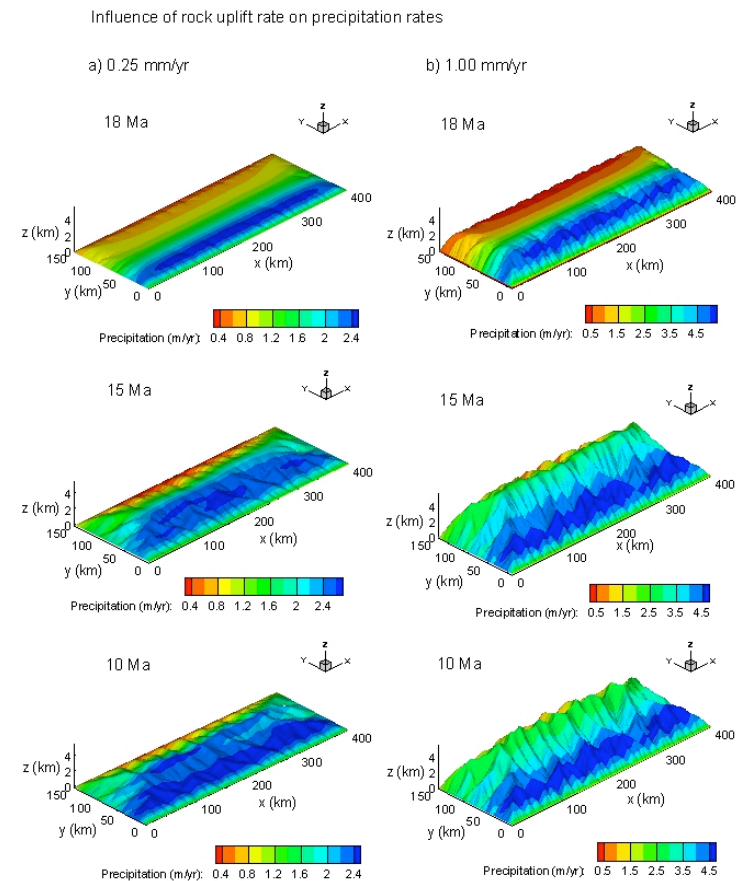
Figure 8. Precipitation rates and distribution across the developing mountain range shows topographic feedbacks on climate (orographic precipitation). Results are shown for the same simulations shown in Figure 2 (simulations m026c and m029c with uplift rates of 0.25 mm/yr and 1.00 mm/yr, respectively).
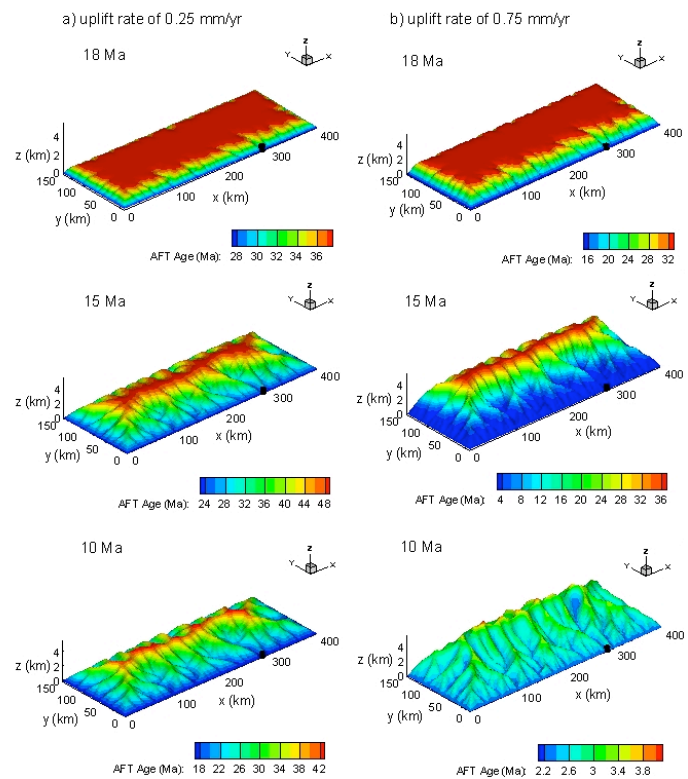
Figure 9. Influence of drainage basin evolution on apatite fission track ages. Compare to Figure 5, which presents the results for apatite helium ages. These plots present the ages of rocks exposed at the surface for three different times and for simulations m026c and m028c with respective exhumation rates of 0.25 and 0.75 mm/yr. The contour scales give a sense of the age ranges eroding off the mountain at the time shown. The black point indicates the position of catchment 1394, which will be considered in the discussion section.